Ann. N.Y. Acad. Sci. ISSN 0077-8923

ANNALS OF THE NEW YORK ACADEMY OF SCIENCES

Original Article

Biomimetic approach to articular cartilage tissue engineering using carbon nanotube–coated and textured polydimethylsiloxane scaffolds

Katrín Lind Elídóttir,[1,2] Louie Scott,[2] Rebecca Lewis,[2] and Izabela Jurewicz[1]

[1]Department of Physics, Faculty of Engineering and Physical Sciences, University of Surrey, Guildford, UK. [2]Department of Veterinary Pre-Clinical Sciences, University of Surrey, Guildford, UK

Address for correspondence: Izabela Jurewicz, Department of Physics, Faculty of Engineering and Physical Sciences, University of Surrey, Stag Hill, Guildford, Surrey GU2 7XH, UK. izabela.jurewicz@surrey.ac.uk; Rebecca Lewis, Department of Veterinary Pre-Clinical Sciences, University of Surrey, Guildford GU2 7AL, UK. rebecca.lewis@surrey.ac.uk

There is a significant need to understand the complexity and heterogeneity of articular cartilage to develop more effective therapeutic strategies for diseases such as osteoarthritis. Here, we show that carbon nanotubes (CNTs) are excellent candidates as a material for synthetic scaffolds to support the growth of chondrocytes—the cells that produce and maintain cartilage. Chondrocyte morphology, proliferation, and alignment were investigated as nanoscale CNT networks were applied to macroscopically textured polydimethylsiloxane (PDMS) scaffolds. The application of CNTs to the surface of PDMS-based scaffolds resulted in an up to 10-fold increase in cell adherence and 240% increase in proliferation, which is attributable to increased nanoscale roughness and hydrophilicity. The introduction of macroscale features to PDMS induced alignment of chondrocytes, successfully mimicking the cell behavior observed in the superficial layer of cartilage. Raman spectroscopy was used as a noninvasive, label-free method to monitor extracellular matrix production and chondrocyte phenotype. Chondrocytes on these scaffolds successfully produced collagen, glycosaminoglycan, and aggrecan. This study demonstrates that introducing physical features at different length scales allows for a high level of control over tissue scaffold design and, thus, cell behavior. Ultimately, these textured scaffolds can serve as platforms to improve the understanding of osteoarthritis and for early-stage therapeutic testing.

Keywords: carbon nanotubes; tissue engineering scaffold; articular cartilage; chondrocytes; Raman spectroscopy

Introduction

Osteoarthritis is a painful disease characterized by the loss of articular cartilage, the smooth tissue covering the ends of bones. The function of articular cartilage is to provide cushioning and frictionless movement at the joint. Osteoarthritis is highly prevalent, currently affecting over 240 million people worldwide.[1] It is essential to consider *in vitro* models of cartilage to study arthritis and test potential therapeutic strategies, reducing the need for extensive animal testing or human trials.

To engineer cartilage *in vitro*, suitable scaffold designs must be considered. It has been established that an effective scaffold should imitate the cells' extracellular matrix (ECM).[2–5] Doing so can improve cell proliferation[5] and ensure the artificially produced tissue has the same characteristics as it would *in vivo*.[4] However, mimicking the structure of the ECM is rarely explored at both the nano and macroscales.[6] This is of utmost importance, especially for articular cartilage, which has a particularly unique structure at these length scales. The ECM of cartilage consists mainly of collagen and proteoglycans (composed of a core protein bonded to glycosaminoglycan (GAG) chains).[2] Aggrecan is a cartilage-specific proteoglycan, containing

doi: 10.1111/nyas.14769

Ann. N.Y. Acad. Sci. 1513 (2022) 48–64 © 2022 The Authors. *Annals of the New York Academy of Sciences* published by Wiley Periodicals LLC on behalf of New York Academy of Sciences.

chondroitin sulfate (CS), a sulfated GAG (sGAG).[7] The biomolecules of cartilage form a fibrous, nanoscale structure, which chondrocytes directly interact with in the cartilage matrix.

On the macroscale, articular cartilage is divided into zones, which vary by the arrangement and alignment of collagen fibers and chondrocytes[8,9]—the cells of cartilage. The induction of chondrocyte alignment has previously been explored by using patterning of proteins atop a substrate to improve cell adhesion in specific patterns.[10,11] However, due to interaction with cells, these proteins do not maintain their integrity with time and cells lose the cue to which they align.[12,13] Alternatively, guiding cell alignment by altering the topographical features of a scaffold surface ensures that the cue to which cells align is maintained for the duration of their culture.[14–18]

Carbon nanotubes (CNTs) have emerged as a promising contender as scaffolds for the production of engineered cartilage.[19–29] This is largely due to their intrinsic ability to provide fibrous nanoscale topography resembling that of the ECM,[19,20,22] simulating the immediate environment that chondrocytes interact with *in vivo*. The addition of nanoscale topography has been shown to increase cell adhesion[19,24] and improve chondrocyte proliferation.[26,30] A higher cell number will ensure that cartilage constructs can be produced more rapidly and reduces the initial sample size required for cell isolation. Moreover, CNTs are less likely to cause inflammation[12] and are more mechanically stable than other naturally derived, more commonly used scaffold materials.[12,23] A common issue of current tissue engineering scaffolds is the dissolution or cell uptake of material, leading to a loss of scaffold structural integrity[31–35] and the production of engineered tissue with properties inferior to native tissue.[36–39]

There have been some studies displaying the promise of scaffolds either fabricated from or supplemented with CNTs. CNT-enriched polycarbonate urethane (CNT/PCU) films demonstrated an enhancement of chondrocyte adhesion and cell density by almost 50% compared to the PCU control, which is attributable to improvements in nanoscale surface roughness.[19] Additionally, surface coating with carboxyl-functionalized single-walled carbon nanotubes (SWNTs-COOH) caused an upregulation in the chondrocytes' collagen and fibronectin gene expression, indicating an improved ability to produce cartilage and increased cell adhesion, respectively.[23] King *et al.*[22] demonstrated that woven textiles made from dry-spun multi-walled carbon nanotube (MWNT) yarns led to the production of key cartilaginous components, including collagen and aggrecan. Bahrami Miyanji *et al.*[28] found that adding SWNTs to a chitosan-gelatin scaffold improved wettability, scaffold stability, and cell viability.

In addition to nanotopographical features, the scaffold's mechanical properties should match that of the cell surroundings *in vivo*, to ensure that the properties of the engineered tissue match that of native tissue.[40–42] The Young's modulus of cartilage has been observed to fall within the range of 2–12 MPa,[43–48] with variations observed due to the age of donor, sample location, and testing parameters. Changes in mechanical properties have been shown to significantly alter cell spreading, proliferation, and chondrogenic gene expression.[40,49,50]

The addition of nanoscale surface topography mimicking the native structure of cartilage has been shown to improve cell growth and production of key cartilaginous components.[19,22–24,26,30] Additionally, controlling the alignment of cells has been rarely explored but shown to be vital to replicate the structure of native cartilage.[10–17] Here, polydimethylsiloxane (PDMS) was used to introduce anisotropic macroscale features to control cellular organization, allowing mimicry of cell shape and alignment as observed in the native cartilage zonal structure. CNTs were utilized in this work to introduce nanoscale topography, and the resulting production of cartilage components was investigated. Additionally, we describe the use of rarely explored Raman spectroscopy as a noninvasive, nondestructive method of biochemical analysis that can be performed *in situ*.

Materials and methods

Materials

Liquid elastomer PDMS consisting of two parts (part A containing vinyl groups and part B with hydrosiloxane groups) was purchased from Farnell (QSil 216 250G, Acc Silicones). Carboxyl-functionalized multi-walled nanotubes (MWNTs-COOH) were obtained from Nanocyl (95% purity, Batch no. 151124). The performance of scaffolds was compared to polyester-based coverslips

(Nunc™ Thermanox™ Coverslips, Thermo Fisher Scientific).

Enzymes for chondrocyte isolation, pronase and collagenase II, were purchased from Gibco, Thermo Fisher. All cell culture reagents, including Dulbecco's Modified Eagle Medium (DMEM), fetal bovine serum (FBS), trypsin, penicillin–streptomycin, and sucrose were purchased from Sigma-Aldrich.

Ethanol (BioUltra, for molecular biology, ≥ 99.8%, Sigma-Aldrich) and acetic acid (glacial, ReagentPlus®, ≥ 99%, Sigma-Aldrich) were used for cell fixation, as described below. The non-ionic surfactant Triton X-100 (Sigma-Aldrich) was used for membrane permeabilization, and bovine serum albumin (BSA; Sigma-Aldrich) was used to block nonspecific binding of antibodies prior to immunofluorescence.

Aggrecan staining was accomplished using an anti-aggrecan antibody (ab3778, Abcam) and a goat anti-mouse secondary antibody (ab150113, Abcam). The nuclei of chondrocytes were stained with the fluorescent dye DAPI (4′,6-diamidino-2-phenylindole, H-1200, VECTASHIELD, Vector Laboratories).

Fabrication of scaffolds

This work explored four types of scaffolds, where the micro and nanoscale features were varied. Microscale features were introduced by the use of textured PDMS (T-PDMS), and the effect of these physical features on chondrocyte behavior was compared to chondrocytes grown on flat PDMS (F-PDMS). CNTs were used to provide nanoscale features, and the effect of CNTs was compared to the respective substrates without the addition of CNTs. The performance of these four scaffolds was compared to an overall control of standard cell culture plastic (Nunc™ Thermanox™ coverslips), referred to as control. A schematic of the different scaffolds used is shown in Figure S1 (online only).

To produce flat and textured PDMS substrates, liquid PDMS was used, consisting of two parts (part A and part B). Upon vigorous mixing of the two resin components in a 10:1 ratio (A:B, respectively) for ∼1 min, the container was placed in a desiccator attached to a vacuum pump for up to an hour to enable the air trapped within the mixture to easily escape. The mixture was then poured either into a flat plastic petri dish, or over a textured mold made of a commercial lenticular lens to produce the different topographies. This was then left for 6 h at room temperature to form a crosslinked network of dimethyl siloxane group. Once set, the PDMS was peeled away from the mold, cut to size, and attached to the bottom of a 24-well plate using liquid PDMS mixture applied to the underside of the scaffold.

To produce CNT-coated scaffolds, MWNTs-COOH were first dispersed in de-ionized (DI) water at a concentration of 0.1 mg mL^{-1}. To obtain a homogeneous dispersion, an ultrasound horn (Branson sonifier 150, Fisher Scientific) was used at an output power of 20 W for 5 min (6 kJ). A spray gun (Futurekart airbrush, 0.3 mm, 7 cc) was used to deposit the CNT dispersion onto substrates in a fine mist. All substrates (F-PDMS, T-PDMS, and control) were sprayed simultaneously, and each time, the spray gun was kept at 20 cm from the surface of the sample at a consistent flow rate of dispersion. For each test, 20 mL of dispersion was deposited per 30 samples (∼40 cm^2 surface area).

Substrate characterization

To determine the suitability of the produced substrates, they were characterized with regard to their nanoscale roughness, transmittance, surface wettability, and stiffness. A stylus profilometer (Dektak 150, Veeco Instruments) was used to obtain the topographical cross section of textured scaffolds and the size of features.

To evaluate the topography and quantify the roughness of substrates, atomic force microscope (AFM) (NTEGRA, NT-MDT, Russia) was used, in semicontact mode at an average set point of 10. Golden silicon probes (NSG01 and NSG10; obtained from NT-MDT) were used, with an average force constant of 14.3 N/m. Root mean square (RMS) roughness was obtained by the software associated with the AFM (NOVA P8 Spectra).

The transmittance of substrates under study was recorded at 550 nm using a UV-visible light spectrophotometer (UV-2501PC, Shimadzu). Wettability of the substrates was measured using drop shape analysis method (DSA25B, Krüss). The static sessile-drop contact angle between DI water and the substrate was recorded by the ADVANCE software.

Chondrocyte isolation and cell culture

Articular cartilage was obtained from the metacarpophalangeal joints of cows from a local abattoir. Chondrocytes were isolated by the enzymatic

digestion of bovine articular cartilage, as previously described.[51] After isolation, 1×10^6 chondrocytes were seeded in a 25-cm^2 cell culture flask for expansion at 37 °C for 2 weeks. Cell culture media consisted of DMEM supplemented with 10% FBS, 1% penicillin/streptomycin, and 80 mM sucrose. To monitor cell health and observe growth rates during culture, optical light microscopy was used (Nikon TS100, Nikon Instruments, Tokyo, Japan).

Chondrocytes were grown for up to 7 days to visualize cell adhesion, morphology, and alignment, and 14 days for analysis using Raman spectroscopy. Cells were fixed prior to characterization. Briefly, media was removed, and the cells washed with phosphate-buffered solution (PBS) two to three times before all liquid was removed and the fixative (99% ethanol and 1% acetic acid) was added. The fixative was left on for 30 min at room temperature before being removed and the substrates washed with PBS.

Immunofluorescence

All fluorescence imaging techniques were performed after fixation, as described above. An upright Nikon Eclipse Ci-S fluorescence microscope (Nikon Instruments) fitted with a Nikon DS-Fi2 camera was used. To enable cell counting on the scaffolds, the nuclei were stained with the fluorescent dye DAPI. The nuclei of the cells were visualized using standard DAPI filters (ex/em: 360/460 nm).

For aggrecan detection, cells were incubated at room temperature with 0.5% Triton X-100 in PBS for 15 min on an orbital shaker (PS-M3D Multi-function 3D Rotator, Grant Instruments) to permeabilize the cells. After washing with PBS, nonspecific binding was blocked using 0.5% BSA in PBS for 1 h at room temperature on an orbital shaker, followed by washing and overnight incubation at 4 °C with a 1:200 dilution of anti-aggrecan antibody. Next, cells were washed before incubation at 4 °C with a 1:500 dilution of goat anti-mouse secondary antibody for 1 hour. After washing with PBS, samples are imaged using an FITC filter (ex/em: 480/535 nm). DAPI was used to counterstain the nuclei.

Scanning electron microscopy

Scanning electron microscopy (SEM) (JSM-7100F, JEOL) was used to investigate cell alignment and the extent of cell interaction with substrates. Before imaging, cells were fixed and left to air dry before a 2 nm layer of gold was deposited by a sputter coater (Emitech K575X, Quorum Technologies) to provide a conductive coating. This is to improve the signal-to-noise ratio during SEM imaging and hence acquire better quality images. Substrates were attached to a metal stub by carbon tape for study.

Raman spectroscopy

A Raman spectrometer (NTEGRA Spectra, NT-MDT) was used in inverted mode to determine the presence of biomolecules related to the intra or extracellular components of chondrocytes. A 473 nm wavelength laser was used with a 60× objective lens. This laser wavelength was selected due to its high energy, resulting in more intense spectra and low autofluorescence, thus making the resulting spectra easy to analyze. For detailed analysis, an 1800/600 grating was applied, resulting in an $\sim$1 cm^{-1} step size. To observe a broader range of wavelengths, a 150/500 grating was applied, resulting in an $\sim$5 cm^{-1} step size.

To determine the contribution from chondrocytes and the ECM material produced, Raman spectra of the scaffolds were obtained to serve as a baseline. For PDMS-based scaffolds, an F-PDMS scaffold was used, prepared as described above. To obtain a prominent CNT signal from the PDMS-CNT baseline, a 20 μL drop of the 0.1 mg mL^{-1} MWNT-COOH/DI-water dispersion was drop-cast onto F-PDMS.

Samples of chondrocytes grown on PDMS-based scaffolds were exposed to the laser for 500 s, during which time the spectra were obtained. Despite the relatively long exposure time, no sample damage was observed as evaluated using optical microscopy. For baselines of scaffold materials, 20-s exposure was sufficient. Finally, when components were scanned atop silicon wafers, such as the cell media and chondrocyte cell suspension, the exposure time was 60 and 120 s, respectively.

Raman spectra obtained from each sample were first baseline-corrected by Baseline Correction with Asymmetric Least Squares Smoothing[52] to remove background signal. Spectra were then normalized by the PDMS peak at 1257 cm^{-1}, as this was identified as being unchanged and unobscured within each data set.

Polarized Raman spectroscopy was made possible by altering the angle of the polarizer placed between the sample and the spectrophotometer.

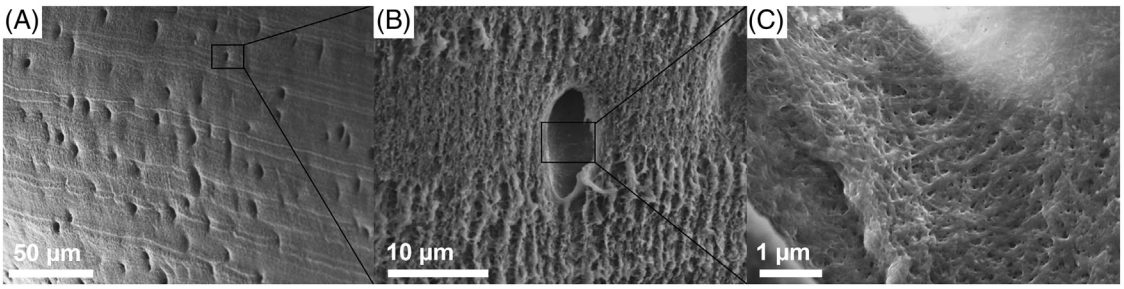

Figure 1. **Scanning electron microscopy (SEM) cross-section images of bovine cartilage. (A) Articular cartilage at 430× magnification. (B) Chondrocyte lacunae at 1800× magnification. (C) Interior of the chondrocyte lacunae at 10,000× magnification. Chondrocytes are absent from the cartilage due to fixation processes.**

This was easily controlled from the software associated with the Raman system (Nova^{TM} software, NT-MDT). So as not to overexpose the sample, spectra were recorded at 30° intervals. Polarized data were fitted on a polar plot using a protocol described in the Supplementary Information (online only).

Statistical analysis

Data were expressed as the mean ± standard deviation. All experiments were repeated at least three times and the statistical significance was determined by single-factor ANOVA, where $P < 0.05$ was considered statistically significant.

Results

Cartilage structure

In order to appropriately design and engineer synthetic scaffolds that mimic the structure of the natural chondrocyte environment, SEM imaging was performed on bovine articular cartilage to observe the detailed structure (Fig. 1). SEM images displayed the organization of cartilage (Fig. 1A), whereby the lacunae (pockets where chondrocytes sit within the ECM matrix) were evident, highlighting the distribution of chondrocyte positioning and organization within the cartilage matrix. A single lacuna was examined (Fig. 1B), where the highly fibrous nature of the ECM was revealed. The fibers surrounding the lacuna were anisotropic and relatively large in diameter (∼0.5 µm). The lacuna appeared elongated parallel to fiber orientation, demonstrating the alignment of chondrocytes with the fibers of the ECM. Conversely, inside the lacuna (Fig. 1C), fibers appeared isotropic and significantly smaller in diameter (∼50–100 nm).

These findings suggest that an appropriate scaffold to support the growth of chondrocytes requires anisotropic features to guide chondrocyte alignment, but with isotropic, nanoscale, fibrous topography. To mimic the nanostructure of ECM, MWNTs-COOH were used in this study, with an average diameter and length of 9.8 nm and 0.78 µm, respectively, as measured by AFM. PDMS-based substrates were studied and polyester-based substrates (referred to herein as plastic based) were used as a control, and both were coated with MWNTs-COOH using spray deposition. The choice of PDMS in this study was dictated by the fact that it is a biologically inert synthetic polymer with mechanical properties closely resembling the mechanical properties of native articular cartilage. The average static elastic modulus of articular cartilage has previously been reported to be in the range of 2–12 MPa.[45–48] The indentation test performed on our substrates revealed the stiffness of pristine PDMS to be 8.7 ± 0.6 MPa, matching that of cartilage (Fig. S2, online only).

Improvement of cell–scaffold interactions by CNT coating

Four different scaffold architectures were prepared in this study: flat (F) and textured (T) PDMS scaffolds (F-PDMS and T-PDMS, respectively) that were either coated with MWNT-COOH (F-PDMS-CNT and T-PDMS-CNT) to enhance their nanoscale characteristics or left uncoated. Three-dimensional (3D) AFM images demonstrate the microscale structure of PDMS without and with CNT coating (Fig. 2A and B, respectively). Where CNT coating was present, entangled fibrous architecture was observed.

Ann. N.Y. Acad. Sci. 1513 (2022) 48–64 © 2022 The Authors. *Annals of the New York Academy of Sciences* published by Wiley Periodicals LLC on behalf of New York Academy of Sciences.

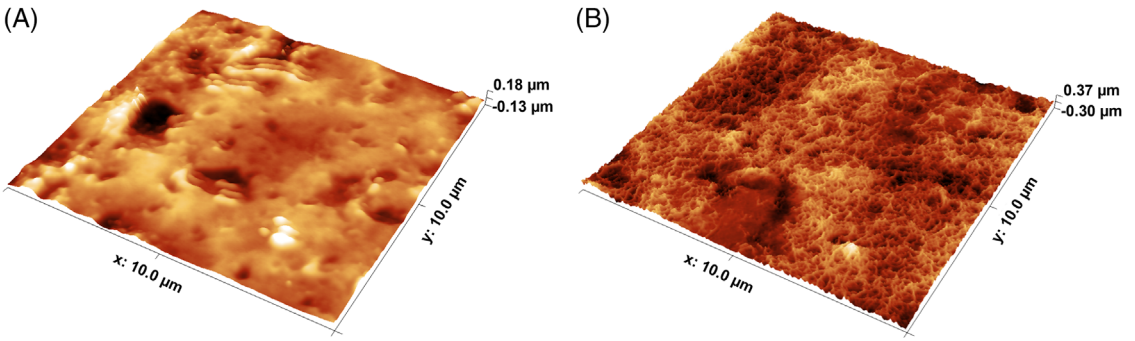

Figure 2. **Representative three-dimensional (3D) AFM topography images displaying the variation in topography at the nano to microscale. (A) F-PDMS, where the smooth PDMS surface is shown with some microscale defects. (B) F-PDMS-CNT showing a network of CNTs atop PDMS.**

The RMS surface roughness of F-PDMS measured by AFM was ∼32 nm, which increased to ∼86 nm after coating with CNTs (Table 1). Both F-PDMS and F-PDMS-CNT substrates showed greater roughness than the control uncoated plastic (∼0.3 nm) and the control coated with CNTs (∼16 nm) (Fig. S3, online only).

The transmittance at 550 nm (T_{550}) of F-PDMS was 93% compared to 86% for the standard cell culture control. The addition of a thin CNT coating reduced T_{550} by only 10% for both the control and F-PDMS. This indicates that the CNT spray deposition method employed was highly reproducible regardless of the type of substrate used.

To examine the wettability of the scaffolds, contact angle measurements were performed by drop shape analysis of water on substrates. The contact angle (θ) of F-PDMS was 112°, which was increased significantly when compared to the control substrate. This was improved by 9° by coating with CNTs, making F-PDMS-CNT more hydrophilic. Similarly, the addition of a CNT coating to cell culture plastic resulted in a decrease of water contact angle yielding a more hydrophilic surface.

Optical microscopy images qualitatively demonstrated the improvements in cell coverage due to the addition of CNT coating (Fig. 3A, D, and G). The control-CNT substrate (Fig. 3A) showed a complete coverage of cells across the entire substrate. The high level of interaction between chondrocytes and CNTs was observed on the control-CNT substrate using SEM (Fig. 3B and C). Chondrocytes can be seen to adhere extremely well, as demonstrated by cells merging with the fibrous CNT-based architecture, the flattening of the chondrocytes' morphology, and the significant presence of dendritic extensions. In comparison, optical microscopy images of F-PDMS (Fig. 3D) show a sparse covering of cells, but more importantly, islands of cells are observed where chondrocytes have clustered together. Chondrocytes grown on F-PDMS show lower interaction with pristine PDMS substrate compared to F-PDMS-CNT (Fig. 3D–F). The chondrocytes' morphology appears rounder, in an attempt to minimize contact with the substrate. However, as PDMS is more flexible than plastic, wrinkling of the surface is observed where dendritic projections from chondrocytes meet the substrate; this wrinkling is absent in the control-CNT sample (Fig. 3C). The issues with low interaction between cells and pristine PDMS are mitigated by the addition of a thin CNT coating on the surface of the F-PDMS-CNT substrate (Fig. 3G–I). The presence of CNTs causes chondrocytes to spread evenly over the entire surface. Interestingly, due to the force exerted by chondrocytes on PDMS substrates, local wrinkling of PDMS occurs regardless of whether the CNTs are present or not (Fig. 3I and F, respectively).

DAPI staining was used to visualize the nuclei of chondrocytes and enable cell counting (Fig. 4A–F). After 1 day of culture on these scaffolds, the differences in chondrocyte number are nonsignificant for all substrates, apart from F-PDMS, which displays a significantly lower cell count (Fig. 4G, 6 ± 3 cells/mm^2 compared to 27–58 cells/mm,^{2} $P < 0.05$). After 3 days in culture, the cell count remains the lowest for F-PDMS (20 ± 11 cells/mm^2),

Table 1. Physical properties of the different scaffolds used

Parameter	Control	Control-CNT	F-PDMS	F-PDMS-CNT
Transmittance T_{550} (%)	86 ± 2	76 ± 2	93 ± 2	83 ± 2
RMS roughness (nm)	0.3 ± 0.1	16 ± 1	32 ± 14	86 ± 18
Water contact angle θ (°)	68 ± 2	48 ± 1	112 ± 1	103 ± 7

followed by T-PDMS (44 ± 19 cells/mm^2), compared to all other scaffolds. However, this is improved by the addition of CNTs (297 ± 52 cells/mm,^{2} $P << 0.05$ for F-PDMS-CNT and 198 ± 55 cells/mm,^{2} $P << 0.05$ for T-PDMS-CNT). Longer term cell culture (7 days) shows the most substantial differences in cell behavior between different scaffold types. There is a significant increase in cell number due to the addition of CNTs onto all substrates, namely, on control-CNT, F-PDMS-CNT, and T-PDMS-CNT compared to their pristine counterparts (150%, 210%, and 240% increase, respectively, $P < 0.05$), which is clearly visible in the fluorescent microscopy images (Fig. 4A–F).

Control of chondrocyte alignment using textured PDMS

With the aim to control cellular organization, PDMS was patterned to produce textured PDMS (T-PDMS). The topography of T-PDMS was explored using confocal microscopy and AFM (Fig. 5A and B, respectively). The average width and height of the grooves were 267 and 36 μm, respectively, as measured by a stylus profilometer. The AFM study revealed a significant increase in the roughness of T-PDMS at the peak of the grooves as opposed to the trough and it is evident that immediately below the peak, this roughness is significantly reduced (Fig. 5B). This increase in roughness was simply due to imperfections between individual lenticules of the mold used, arising from manufacturing limitations. When PDMS is cast on top of this mold and subsequently removed after crosslinking, its surface texture is directly transferred onto the molded substrate.

Optical micrographs (Fig. 5C) show that using T-PDMS as cell scaffolds resulted in a significant alignment of cells on top of the grooves. Chondrocytes align in the direction of the features introduced by molding of PDMS, using contact guidance.[53] Moreover, there is a significantly greater cell number at the peaks of these features compared to the troughs. SEM images allow insights into cell morphology (Fig. 5D), where chondrocytes on T-PDMS appear elongated in the direction of the grooves. High magnification SEM imaging shows cell–substrate interactions with T-PDMS (Fig. 5E), where wrinkling is observed at the surface of the substrates, as was seen with F-PDMS.

The alignment of chondrocytes was mitigated when CNTs were added, as in the case of the T-PDMS-CNT scaffold (Fig. 5F–H). Optical micrographs show the vast difference in cell distribution compared to T-PDMS, whereby cells are found equally distributed on the peaks and troughs of the textured scaffold. The cells are randomly oriented, and overall cell density has vastly increased with the addition of CNTs. A flatter cell morphology was observed for chondrocytes grown on T-PDMS-CNT when compared to pristine T-PDMS (Fig. 5G). Dendritic extensions protruded from cells in several directions, as opposed to the pristine scaffold, where they were found to extend parallel to the features of the textured scaffold. Wrinkling was observed where the cell meets the scaffold surface (Fig. 5H). SEM, optical microscopy, and fluorescence microscopy for aggrecan were utilized to visualize and further highlight chondrocyte alignment (Fig. 6A–C).

Identification of cartilage components using Raman spectroscopy

Raman spectroscopy was used to assess ECM material produced by chondrocytes cultured on the scaffolds after 2 weeks (Fig. 7). Cells successfully produced all constituent biomolecules of cartilage, namely, collagen (at 898, 1231, 1254, 1289, 1356, and 1468 cm^{-1}),[9,54–57] GAG (1379 and 1408 cm^{-1}),[9,55] and CS (1058 and 1280 cm^{-1}),[9,22,54,55] which is present in the cartilage-specific proteoglycan aggrecan (comprehensive Raman peak assignments for all scaffolds under study are shown in Table S1, online only). There were some nonspecific proteins identified at 1120 cm,$^{-1}$ [55–57] and the

Ann. N.Y. Acad. Sci. 1513 (2022) 48–64 © 2022 The Authors. *Annals of the New York Academy of Sciences* published by Wiley Periodicals LLC on behalf of New York Academy of Sciences.

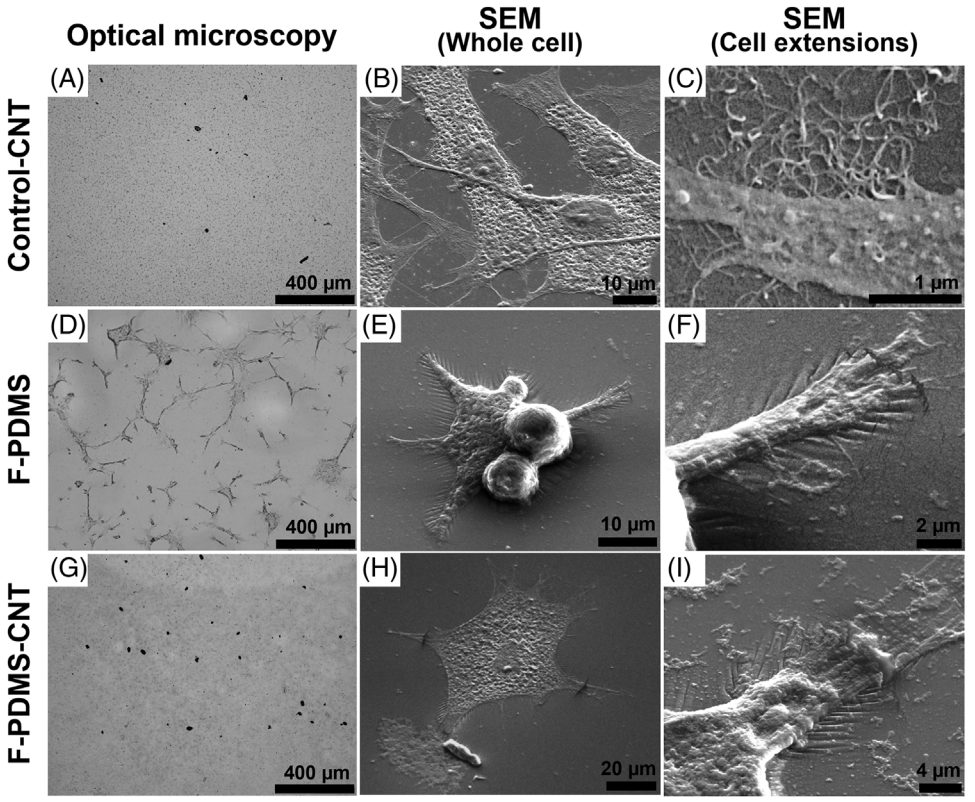

Figure 3. **Optical microscopy images taken after 7 days of culture (left) and SEM micrographs taken after 3 days of culture (middle and right) of chondrocytes grown on control-CNT (A–C), F-PDMS (D–F), and F-PDMS-CNT (G–I).**

amino acid phenylalanine was observed at 1004 cm^{-1}.[9,54,57] The most significant contributions to this spectrum were associated with DNA (1094 cm^{-1}),[56] indicating that the Raman spectrum in this instance was obtained at the nucleus of a cell. A representative spectrum is shown in Figure 7A; the spectra obtained for all scaffolds under study can be found in Figure S4 (online only), with associated peak assignments.

Control of collagen fiber alignment using textured PDMS

Polarized Raman spectroscopy was used on the PDMS-based scaffolds to examine the alignment of collagen fibers by analyzing the polarization dependence of the Raman peak at 1356 cm^{-1}, which is attributable to collagen wagging.[58,59] Polarized Raman spectra were obtained as a function of polarization angle from 0° to 330° from cells grown on pristine T-PDMS (Fig. S5, online only). There was a clear increase in intensity observed at a polarization angle of 90° and 270°, with the intensity being at its lowest at 0° and 180° (Fig. 7B). This corresponds to the collagen molecules of the sample aligning perpendicularly to the polarization of the laser beam. This was established by obtaining the depolarization ratio (ρ), which is defined as the ratio of the intensity of the depolarized to the polarized component (Eq. (2) in the Supporting Information, online only), where polarization dependence is defined as $\rho < 0.75$.[60] For T-PDMS, a depolarization ratio of $\rho = 0.46$ was found, confirming the alignment of collagen fibers on this substrate. This is highlighted by the radial plot produced by obtaining the intensity for the 1356 cm^{-1} peak at each angle of polarization. For an anisotropic distribution, the fitting produces the oblong shape observed here, whereas an isotropic distribution results in a circular plot.

As chondrocyte alignment was lost with the addition of spray-coated CNTs, the spectra of chondrocytes grown on T-PDMS were compared to that of T-PDMS-CNT and F-PDMS-CNT to

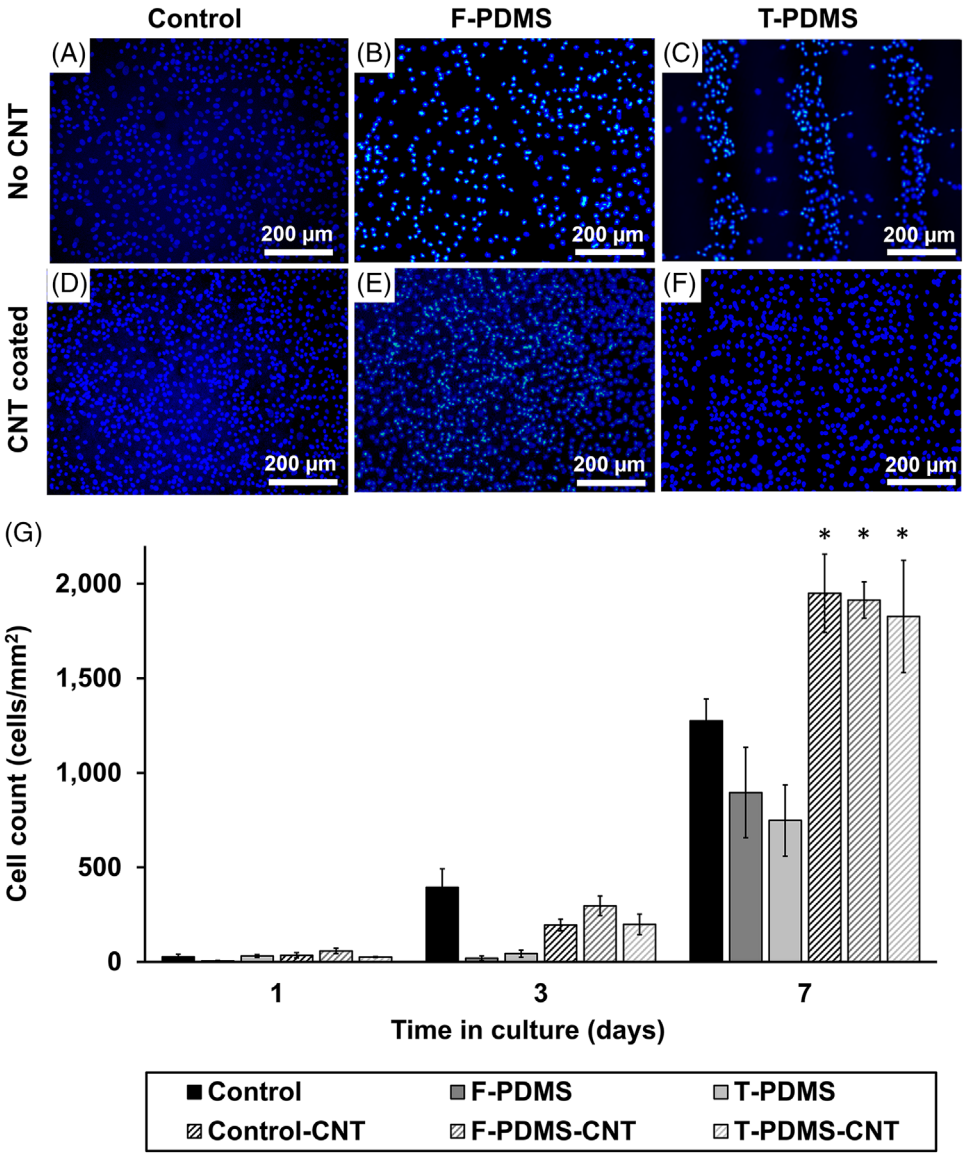

Figure 4. Representative DAPI fluorescence microscopy images of all substrates after 7 days of cell culture. (A) Control. (B) F-PDMS. (C) T-PDMS. (D) Control-CNT. (E) F-PDMS-CNT. (F) T-PDMS-CNT. (G) Cell count per unit area is displayed for 1, 3, and 7 days of cell culture on each scaffold type. $^*P < 0.05$, compared to control.

investigate the resulting changes in collagen alignment (Figs. S6 and S7, online only). The intensity of the collagen peak of the T-PDMS-CNT polar plot appeared random with respect to polarization angle (Fig. 7C). When the data were fitted, the average depolarization ratio $\rho = 0.75$ was obtained, corresponding to a lack of alignment, although the depolarization ratio is on the border differentiating alignment from isotropic arrangement, indicating that perhaps the textured features play some role in the alignment of collagen. Similarly, the collagen contribution observed at 1356 cm^{-1} on F-PDMS-CNT shows that intensity is not dependent on polarization (Fig. 7D), as confirmed by a depolarization ratio of fitted data of $\rho \sim 1$, indicating a lack of alignment of collagen fibers.

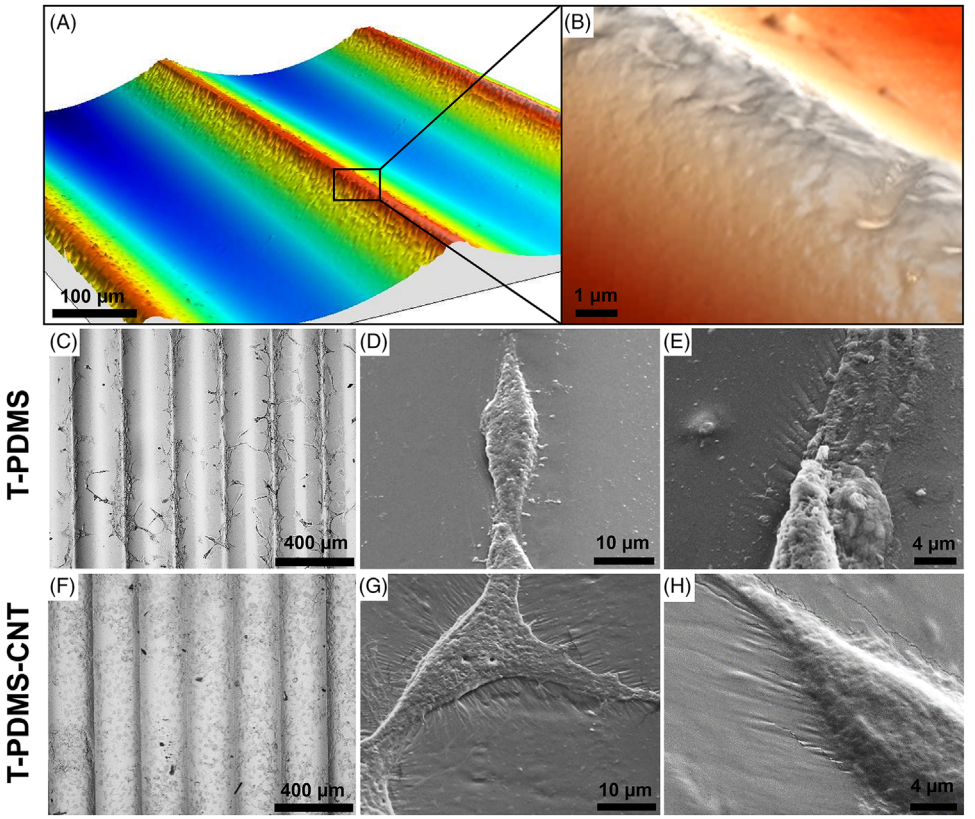

Figure 5. (A) A confocal microscopy image displaying the 3D macroscale topography of T-PDMS. (B) A 3D topography AFM image showing the nano to microscale topography of T-PDMS, highlighting the increased roughness on the peak of the grooves. Optical microscopy images taken after 7 days of culture (left) and SEM micrographs taken after 3 days of culture (middle and right) of chondrocytes on T-PDMS (C–E) and T-PDMS-CNT (F–H).

Discussion

This study demonstrates that the behavior of chondrocytes can be influenced by the topography of their underlying substrate. First, we observe that roughness is a key parameter in improving cell adhesion to PDMS and that the addition of CNTs atop PDMS produces an isotropic fibrous architecture and hence an enhanced roughness. This mimics the combination of nano and microscale structure seen in native cartilage. CNTs provide a higher relative surface area, and, thus, more points of adhesion for cellular proteins, aiding cell adhesion. Improving cell adhesion, in turn, improves growth conditions for cells, encouraging proliferation and the production of cartilage-specific ECM.[26,30] It is vital to improve upon the growth rates of chondrocytes, as osteoarthritic patients must currently wait up to 6 weeks for autologous chondrocyte expansion alone, so an improvement of 150–240% is incredibly significant in being able to improve quality of life sooner. Additionally, the substrates used can help provide a platform for testing of emerging osteoarthritis therapies. Animal testing is currently considered an essential part of arthritis research—rules set by the home office state that animals can only be used where there is no alternative.[61] Providing a viable alternative platform for testing will, therefore, reduce the need for animal testing.

MWNTs-COOH were selected here to mimic the fibrous architecture of the ECM. The choice of the type of CNTs was dictated by their dispersibility in water, without the need for organic solvents or stabilizing agents, such as surfactants, that are widely cytotoxic.[62,63] Moreover, the presence of the carboxyl (COOH) functional groups on a substrate has been demonstrated to improve cell adhesion. It is well established that the COOH group

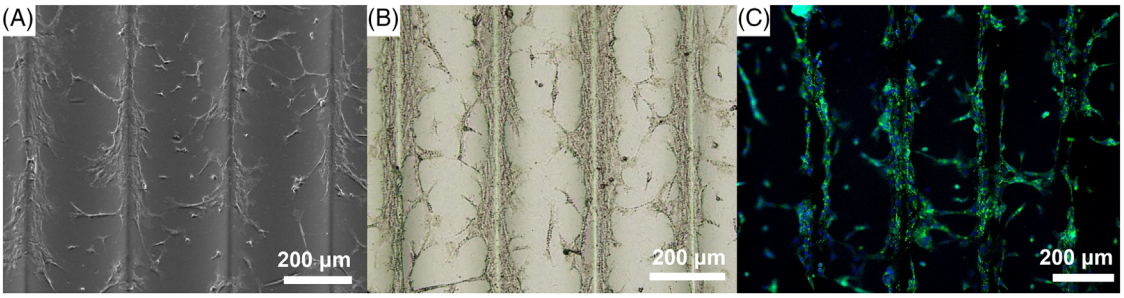

Figure 6. **Alignment of chondrocytes along the peaks of T-PDMS demonstrated through various microscopy techniques: (A) SEM, (B) brightfield optical microscopy, and (C) aggrecan staining of chondrocytes, counterstained with DAPI (green and blue fluorescence, respectively).**

self-associates in solution. A proton is donated from the hydroxyl (OH) group, creating a negative charge at the surface. This alters the surface charge, which is a known controlling factor of cell adhesion and biocompatibility,[64] as it mimics the negative charge of ECM molecules, such as the sulfate and carboxyl groups of proteoglycans—the second largest group of biomolecules within cartilage.[23]

High optical transparency is a key attribute of a successful tissue scaffold since it enables the visualization of cell culture using readily available optical microscopy techniques. All PDMS-based scaffolds showed optical transmittance comparable, if not improved relative to the control. This is due to greater innate optical properties of PDMS compared to standard cell culture plastic. This demonstrates that PDMS-based substrates are optimal for chondrocyte culture in any standard lab, without the need for specialized equipment to observe cell growth and health.

PDMS possesses the ideal mechanical properties for a chondrocyte scaffold as they resemble the mechanical properties of native articular cartilage. However, its poor wetting properties lead to a diminished number of cells observed on its surface. Chondrocytes were observed to form clusters in order to minimize cellular contact with the substrate due to poor affinity with its surface. Scaffolds, including PDMS, are usually modified with the protein fibronectin to enable efficient cellular attachment.[65] Organic materials, however, can increase the risk of infection as they are more likely to promote bacterial adhesion and colonization;[66–68] therefore, our scaffolds were coated with wholly synthetic CNTs instead. The addition of CNTs to the surface of PDMS led to a ∼10% improvement in wettability. As a result, chondrocytes displayed a higher affinity for the scaffold surface. Local wrinkling of PDMS occurs (with and without the addition of CNTs), where dendritic projections from chondrocytes meet the surface of the substrate. This is due to cell-generated stresses (traction forces) leading to substrate deformation.[69,70] Chondrocytes utilize a process called mechanotransduction to sense the stiffness of the underlying material onto which they are seeded.[71] Mechanotransduction is the transformation of a mechanical stimulus detected by cells into a chemical response. Therefore, the ability of a substrate to deform is imperative in cartilage tissue engineering. Cells are only able to exert force onto a substrate once adhesion proteins interact with the substrate. There is no evidence of traction forces on the control coated with CNTs, as this substrate is too stiff, limiting the ability of cells to deform and interact with the substrate.

Choosing between textured PDMS and flat PDMS coated with CNTs provides the ability to control the distribution and density of chondrocytes, which is crucial for the biomimicry of native cartilage. The architecture of cartilage is highly complex and is organized into different zones that vary by chondrocyte and fiber alignment. To successfully mimic each of the different zones of cartilage, it is vital to be able to control the organization of chondrocytes. For example, the type of cell arrangement observed on F-PDMS-CNT, where chondrocytes are isotropically distributed, most closely resembles the middle zone of the cartilage. In the superficial zone of cartilage, cells are aligned perpendicular to the surface of the joint, providing a smooth surface for movement. The anisotropic

Ann. N.Y. Acad. Sci. 1513 (2022) 48–64 © 2022 The Authors. *Annals of the New York Academy of Sciences* published by Wiley Periodicals LLC on behalf of New York Academy of Sciences.

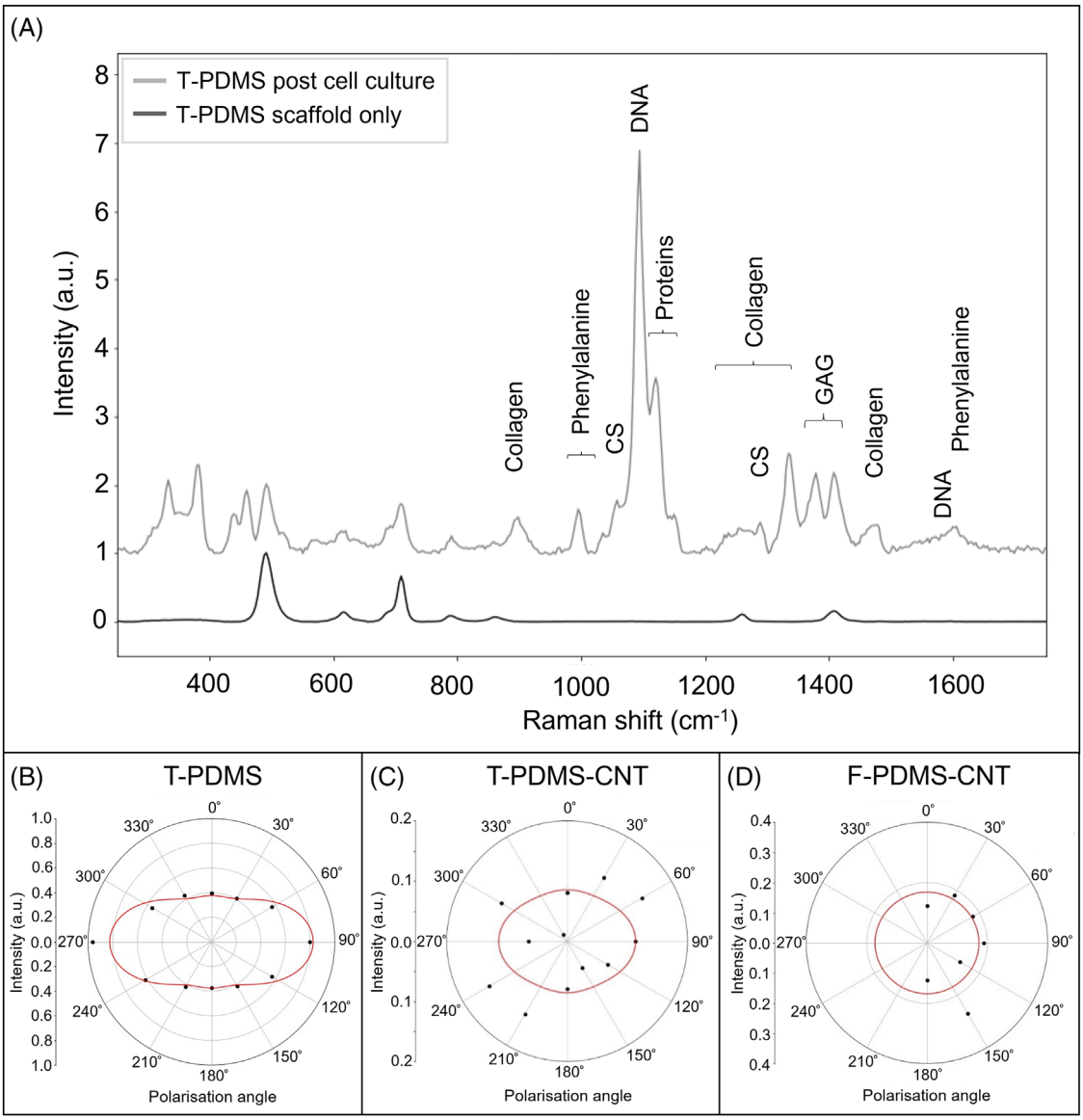

Figure 7. **Representative Raman spectra of T-PDMS substrates after 14 days of chondrocyte culture. (A) T-PDMS substrate (black) and T-PDMS seeded with chondrocytes (gray). Polarized Raman spectra were obtained and then the intensity of the collagen peak at 1356 cm^{-1} was plotted as a function of polarization angle from 0° to 330° for cells grown on: (B) T-PDMS, (C) T-PDMS-CNT, and (D) F-PDMS-CNT.**

arrangement of chondrocytes can be induced using textured PDMS, where the presence of macroscopic physical features triggers the alignment of chondrocytes along the peaks of the grooves. To our knowledge, there are no reports in the literature showing the behavior displayed here, where chondrocytes align at the peak of features. When grooved patterning had been used previously for chondrocytes, the groove width was significantly narrower than the cell width.[14,16,22] This was done with the aim of guiding subcellular components, such as dendritic extensions, focal adhesions, and actin filaments. However, this is often inconsistent as cells are able to grow across and beyond the patterns, which are smaller than the average width of the cells themselves. Conversely, when cell alignment

has been attempted with patterns wider than cell size, it has been with the purpose of providing constraints. Thus, cells align between the peaks of the patterns, as opposed to along the peaks,[72–74] and cell alignment was observed in the concave part of the feature.[73–76] The unusual assembly of chondrocytes on top of the grooves arises from an increase in the roughness of the peak of the grooves compared to the troughs. We have established here that surface roughness has a key function in cell attachment. Since the tops of the grooves are rougher than the base of the grooves, this is likely the reason for the preferential growth and improved growth rate of chondrocytes on the uppermost part of the textured PDMS scaffolds. Then, using contact guidance, chondrocytes align against the macroscopic features of the grooves. Chondrocytes elongate and stretch parallel to the length of the peaks, whereas at the troughs, they are rounder. This is the same behavior observed on F-PDMS, whereby the rounder morphology is caused by the cell minimizing contact with an unsuitable surface.

It must be noted that although the enhanced surface roughness of PDMS is advantageous for the cells' attachment, nanoscale roughness can be applied in a more controlled and tunable manner using CNTs. CNTs have the additional advantage of resembling fibrous ECM that is so important in *in vivo* conditions, as well as being electrically conductive (Fig. S8, online only). Although outside the scope of the work presented here, it has been previously suggested that electrical stimulation of chondrocytes is beneficial to their proliferation.[19,77] This further highlights the functionality of these PDMS-based scaffolds decorated with a conductive, nanofibrous CNT network.

Chondrocytes are commonly grown to expand their number for implantation or *in vitro* cartilage formation. However, during this process, chondrocytes commonly lose their phenotype.[78] This means they are no longer able to produce cartilage-specific biomolecules, such as aggrecan, and can, therefore, not maintain or form cartilage tissue. Immunofluorescence analysis of aligned cells suggests that there is a high expression of aggrecan, demonstrating that textured PDMS supports the growth of healthy, cartilage-producing chondrocytes. As well as confirming the presence of aggrecan, it is vital to analyze the production of cartilage components. Raman spectroscopy reveals here that key cartilage components were successfully produced on all scaffolds investigated in this study, namely, the presence of collagen and CS, an sGAG chain found in aggrecan, demonstrating that these scaffolds are capable of successfully forming cartilage *in vitro*.

During long-term culture of chondrocytes, it is also a common issue that they will deposit hydroxyapatite ($Ca_{10}(PO_4)_6(OH)_2$), a calcium phosphate mineral found in bone and calcified cartilage, but not in hyaline cartilage. Calcified cartilage is found between hyaline cartilage and the bone in joints, and it is also made up of and maintained by chondrocytes. However, it does not have the appropriate structure or mechanical properties to provide the same function as hyaline cartilage in the joint. This work shows that Raman spectroscopy is the ideal tool to indicate whether scaffolds encourage the production of hyaline or calcified cartilage. Chondrocytes grown for 2 weeks on the scaffolds produced here showed no markers of calcified cartilage. Additionally, the OSO_3^- symmetric stretch peak ($\sim$1060 cm^{-1}) arising from the cartilage-specific proteoglycan aggrecan has been shown to be absent in the Raman spectra of calcified cartilage.[57] Our Raman investigations clearly show the presence of this OSO_3^- peak, further highlighting the potential for these scaffolds to specifically produce hyaline cartilage.

Raman spectroscopy was also used as a tool to evaluate the alignment of collagen, the most prevalent component of cartilage. Our polarized Raman spectroscopy examination indicates a preferential alignment of collagen fibers parallel to chondrocytes, as is observed in the superficial zone of cartilage *in vivo*. This is an important finding with regard to the mimicking of cartilage zones, which vary by chondrocyte and collagen alignment.[9] There is no evidence of an innate polarization dependence of the wagging mode of collagen, as the movement of the vibration is asymmetric.[79,80] Therefore, the polarization dependence exhibited by the collagen detected is a clear indication of the alignment of collagen fibers on textured PDMS. Significantly, these results indicate that the use of textured PDMS enables the control of both chondrocytes and collagen fiber alignment. As chondrocyte alignment can be negated by the addition of CNTs, this enables to reproduce different zones of cartilage in a highly controlled fashion.

Ann. N.Y. Acad. Sci. 1513 (2022) 48–64 © 2022 The Authors. *Annals of the New York Academy of Sciences* published by Wiley Periodicals LLC on behalf of New York Academy of Sciences.

Conclusion

We have demonstrated the need for nanostructured scaffolds to mimic the ECM of chondrocytes in order to improve the quality of resulting cartilage constructs. This work outlines ways in which physical properties of tissue engineering scaffolds can be altered to control cell behavior, including proliferation and alignment. A substantial increase in nanolevel roughness (∼270% increase by the addition of CNT coating on PDMS-based scaffolds) was found to improve cell adhesion. It was also possible to control the direction of growth of chondrocytes by the introduction of micro-sized anisotropic features without the presence of CNTs. In the presence of randomly arranged CNTs, the cells cease to conform to microscale features. This implies that cells preferentially take cues regarding their alignment from nanoscale topography. To our knowledge, the cell behavior of aligning at the peaks of macroscale features has never been reported before. This provides fundamental knowledge to the field of tissue engineering for the design of smart scaffolds. These initial results indicate that the system has excellent biocompatibility, with chondrocytes proliferating on and interacting with all PDMS-CNT substrates.

Acknowledgments

This work was supported by the Doctoral College and the Department of Physics at the University of Surrey, and by the Longhurst Legacy awarded to the School of Veterinary Medicine, as well as the Faculty of Health and Medical Sciences research support fund. The authors would like to thank Violeta Doukova and Agata Gajewicz-Jaromin for their laboratory assistance. We thank Zhendong (Fisher) Yu for assistance in developing the textured scaffold protocol.

Author contributions

K.L.E. was responsible for the conceptualization, data acquisition, analysis, interpretation, and drafting of the manuscript. L.S. was responsible for conceptualization and manuscript reviewing and editing. R.L. and I.J. were responsible for conceptualization, design, data interpretation, and manuscript reviewing and editing.

Supporting information

Additional supporting information may be found in the online version of this article.

Figure S1. Schematic of the four scaffolds examined in this work and two controls displaying the structural differences.

Figure S2. Representative force-displacement curve for PDMS-based substrates.

Figure S3. 3D AFM images of plastic-based substrates.

Figure S4. Raman spectra of all substrates under study.

Figure S5. (A) Spectra for polarized Raman spectroscopy of T-PDMS with cells grown for 2 weeks. (B) Intensity of collagen peak at 1356 cm^{-1} for polarized spectra for T-PDMS and cells.

Figure S6. (A) Spectra for polarized Raman spectroscopy of T-PDMS-CNT with cells grown for 2 weeks. (B) Intensity of collagen peak at 1356 cm^{-1} for polarized spectra shown for T-PDMS-CNT and cells.

Figure S7. (A) Spectra for polarized Raman spectroscopy of F-PDMS-CNT with cells grown for 2 weeks. (B) Intensity of collagen peak at 1356 cm^{-1} for polarized spectra shown for F-PDMS-CNT and cells.

Figure S8. Log-linear graph of the change in sheet resistance (R_S) as a function of the density of the CNT network, as represented by a change in optical transmittance at 550 nm (T_{550}).

Table S1. Raman peak positions and their respective molecular and vibrational assignment.

Competing interests

The authors declare no competing interests.

References

1. Vos, T., R.M. Barber, B. Bell, *et al.* 2015. Global, regional, and national incidence, prevalence, and years lived with disability for 301 acute and chronic diseases and injuries in 188 countries, 1990–2013: a systematic analysis for the Global Burden of Disease Study 2013. *Lancet* **386:** 743–800.
2. Lim, E.-H., J.P. Sardinha & S. Myers. 2014. Nanotechnology biomimetic cartilage regenerative scaffolds. *Arch. Plast. Surg.* **41:** 231–240.
3. Heister, E., E.W. Brunner, G.R. Dieckmann, *et al.* 2013. Are carbon nanotubes a natural solution? Applications in

biology and medicine. *ACS Appl. Mater. Interfaces* **5:** 1870–1891.
4. Duarte Campos, D.F., W. Drescher, B. Rath, *et al.* 2012. Supporting biomaterials for articular cartilage repair. *Cartilage* **3:** 205–221.
5. Cai, S., H. Xu, Q. Jiang, *et al.* 2013. Novel 3D electrospun scaffolds with fibers oriented randomly and evenly in three dimensions to closely mimic the unique architectures of extracellular matrices in soft tissues: fabrication and mechanism study. *Langmuir* **29:** 2311–2318.
6. Brunner, E.W., I. Jurewicz, E. Heister, *et al.* 2014. Growth and proliferation of human embryonic stem cells on fully synthetic scaffolds based on carbon nanotubes. *ACS Appl. Mater. Interfaces* **6:** 2598–2603.
7. Hall, B.K. 2015. Invertebrate cartilages, notochordal cartilage and cartilage origins. In *Bones and Cartilage*. 63–78. Academic Press.
8. Stevens, M.M., H.F. Qanadilo, R. Langer, *et al.* 2004. A rapid-curing alginate gel system: utility in periosteum-derived cartilage tissue engineering. *Biomaterials* **25:** 887–894.
9. Bergholt, M.S., J.P. St-Pierre, G.S. Offeddu, *et al.* 2016. Raman spectroscopy reveals new insights into the zonal organization of native and tissue-engineered articular cartilage. *ACS Cent. Sci.* **2:** 885–895.
10. Pan, C., B. Zhang, M. Zhang, *et al.* 2014. Effects of BMP-2 patterns on bovine chondrocytes adhesion and alignment. *J. Wuhan Univ. Technol. Mater. Sci. Ed.* **29:** 1057–1062.
11. Pan, C.J., H.Y. Ding & Y.X. Dong. 2013. Extracellular matrix protein patterns guide human chondrocytes adhesion and alignment characterized by vimentin and matrilin-3. *Colloids Surf. B: Biointerfaces* **102:** 730–736.
12. Hirata, E., M. Uo, H. Takita, *et al.* 2011. Multiwalled carbon nanotube-coating of 3D collagen scaffolds for bone tissue engineering. *Carbon* **49:** 3284–3291.
13. Inzana, J.A., D. Olvera, S.M. Fuller, *et al.* 2014. 3D printing of composite calcium phosphate and collagen scaffolds for bone regeneration. *Biomaterials* **35:** 4026–4034.
14. Accardi, M.A., S.D. McCullen, A. Callanan, *et al.* 2013. Effects of fiber orientation on the frictional properties and damage of regenerative articular cartilage surfaces. *Tissue Eng. Part A* **19:** 2300–2310.
15. Almeida, H.V., B.N. Sathy, I. Dudurych, *et al.* 2017. Anisotropic shape-memory alginate scaffolds functionalized with either type I or type II collagen for cartilage tissue engineering. *Tissue Eng. Part A* **23:** 55–68.
16. Owida, H.A., R. Yang, L. Cen, *et al.* 2018. Induction of zonal-specific cellular morphology and matrix synthesis for biomimetic cartilage regeneration using hybrid scaffolds. *J. R. Soc. Interface* **15:** 20180310.
17. Romereim, S.M., N.H. Conoan, B. Chen, *et al.* 2014. A dynamic cell adhesion surface regulates tissue architecture in growth plate cartilage. *Development* **141:** 2085–2095.
18. Nakatani, S., M. Sekino, H. Ohsaki, *et al.* 2015. *Control of fiber alignment in collagen gel by static magnetic field and effect of that on ECM synthesis of articular chondrocytes*.
19. Khang, D., G.E. Park & T.J. Webster. 2008. Enhanced chondrocyte densities on carbon nanotube composites: the combined role of nanosurface roughness and electrical stimulation. *J. Biomed. Mater. Res. Part A* **86:** 253–260.
20. Das, K., A. Madhusoodan, B. Mili, *et al.* 2017. Functionalized carbon nanotubes as suitable scaffold materials for proliferation and differentiation of canine mesenchymal stem cells. *Int. J. Nanomed.* **12:** 3235–3252.
21. Vardharajula, S., S.Z. Ali, P.M. Tiwari, *et al.* 2012. Functionalized carbon nanotubes: biomedical applications. *Int. J. Nanomed.* **7:** 5361–5374.
22. King, A.A.K., B. Matta-Domjan, M.J. Large, *et al.* 2017. Pristine carbon nanotube scaffolds for the growth of chondrocytes. *J. Mater. Chem. B* **5:** 8178–8182.
23. Chahine, N.O., N.M. Collette, C.B. Thomas, *et al.* 2014. Nanocomposite scaffold for chondrocyte growth and cartilage tissue engineering: effects of carbon nanotube surface functionalization. *Tissue Eng. Part A* **20:** 2305–2315.
24. Antonioli, E., A.O. Lobo, M. Ferretti, *et al.* 2013. An evaluation of chondrocyte morphology and gene expression on superhydrophilic vertically-aligned multi-walled carbon nanotube films. *Mater. Sci. Eng. C* **33:** 641–647.
25. Janssen, L., M. Saranya, M. Leinonen, *et al.* 2020. Vertically aligned carbon nanotube micropillars induce unidirectional chondrocyte orientation. *Carbon* **158:** 681–689.
26. Gao, Y., S. Liu, J. Huang, *et al.* 2014. The ECM–cell interaction of cartilage extracellular matrix on chondrocytes. *BioMed Res. Int.* **2014:** 648459.
27. Liu, H., J. Chen, S. Qiao, *et al.* 2021. Carbon-based nanomaterials for bone and cartilage regeneration: a review. *ACS Biomater. Sci. Eng.* **7:** 4718–4735.
28. Bahrami Miyanji, P., D. Semnani, A. Hossein Ravandi, *et al.* 2022. Fabrication and characterization of chitosan-gelatin/single-walled carbon nanotubes electrospun composite scaffolds for cartilage tissue engineering applications. *Polym. Adv. Technol.* **33:** 81–95.
29. Szymański, T., A.A. Mieloch, M. Richter, *et al.* 2020. Utilization of carbon nanotubes in manufacturing of 3D cartilage and bone scaffolds. *Materials* **13:** 4039.
30. Terpstra, L., J. Prud'Homme, A. Arabian, *et al.* 2003. Reduced chondrocyte proliferation and chondrodysplasia in mice lacking the integrin-linked kinase in chondrocytes. *J. Cell Biol.* **162:** 139–148.
31. Dong, C. & Y. Lv. 2016. Application of collagen scaffold in tissue engineering: recent advances and new perspectives. *Polymers* **8:** 42.
32. Mirmusavi, M.H., P. Zadehnajar, D. Semnani, *et al.* 2019. Evaluation of physical, mechanical and biological properties of poly 3-hydroxybutyrate-chitosan-multiwalled carbon nanotube/silk nano-micro composite scaffold for cartilage tissue engineering applications. *Int. J. Biol. Macromol.* **132:** 822–835.
33. Sahoo, S., J.G. Cho-Hong & T. Siew-Lok. 2007. Development of hybrid polymer scaffolds for potential applications in ligament and tendon tissue engineering. *Biomed. Mater.* **2:** 169–173.
34. Sahoo, S., H. Ouyang, C.H. James, *et al.* 2006. Characterization of a novel polymeric scaffold for potential application in tendon/ligament tissue engineering. *Tissue Eng.* **12:** 91–99.
35. Elsawy, M.A., K.H. Kim, J.W. Park, *et al.* 2017. Hydrolytic degradation of polylactic acid (PLA) and its composites. *Renew. Sustain. Energy Rev.* **79:** 1346–1352.

36. Nakagawa, Y., S. Mukai, Y. Setoguchi, *et al.* 2017. Clinical outcomes of donor sites after osteochondral graft harvest from healthy knees. *Orthopaed. J. Sports Med.* **5:** 1–6.
37. McCarthy, H.S., J.B. Richardson, J.C.E. Parker, *et al.* 2016. Evaluating joint morbidity after chondral harvest for autologous chondrocyte implantation (ACI): a study of ACI-treated ankles and hips with a knee chondral harvest. *Cartilage* **7:** 7–15.
38. Medvedeva, E.V., E.A. Grebenik, S.N. Gornostaeva, *et al.* 2018. Repair of damaged articular cartilage: current approaches and future directions. *Int. J. Mol. Sci.* **19:** 2366.
39. Silver, F.H. & A.I. Glasgold. 1995. Cartilage wound healing. An overview. *Otolaryngol. Clin. North Am.* **28:** 847–864.
40. Izadifar, Z., X. Chen & W. Kulyk. 2012. Strategic design and fabrication of engineered scaffolds for articular cartilage repair. *J. Funct. Biomater.* **3:** 799–838.
41. Saludas, L., S. Pascual-Gil, F. Prósper, *et al.* 2017. Hydrogel based approaches for cardiac tissue engineering. *Int. J. Pharm.* **523:** 454–475.
42. Holmes, B., X. Fang, A. Zarate, *et al.* 2016. Enhanced human bone marrow mesenchymal stem cell chondrogenic differentiation in electrospun constructs with carbon nanomaterials. *Carbon* **97:** 1–13.
43. Jurvelin, J.S., M.D. Buschmann & E.B. Hunziker. 1997. Optical and mechanical deformation of Poisson's ratio of adult bovine humeral articular cartilage. *J. Biomech.* **30:** 235–241.
44. Treppo, S., H. Koepp, E.C. Quan, *et al.* 2000. Comparison of biomechanical and biochemical properties of cartilage from human knee and ankle pairs. *J. Orthopaed. Res.* **18:** 739–748.
45. Korhonen, R.K., M.S. Laasanen, J. Toyras, *et al.* 2002. Comparison of the equilibrium reponse of AC in unconfined compression and indentation. *J. Biomech.* **35:** 903–909.
46. Woodfield, T.B.F., J. Malda, J. De Wijn, *et al.* 2004. Design of porous scaffolds for cartilage tissue engineering using a three-dimensional fiber-deposition technique. *Biomaterials* **25:** 4149–4161.
47. Shepherd, D.E.T. & B.B. Seedhom. 1999. Thickness of human articular cartilage in joints of the lower limb. *Ann. Rheum. Dis.* **58:** 27–34.
48. Setton, L.A., D.M. Elliott & V.C. Mow. 1999. Altered mechanics of cartilage with osteoarthritis: human osteoarthritis and an experimental model of joint degeneration. *Osteoarthritis Cartilage* **7:** 2–14.
49. Chen, C., J. Xie, L. Deng, *et al.* 2014. Substrate stiffness together with soluble factors affects chondrocyte mechanoresponses. *ACS Appl. Mater. Interfaces* **6:** 16106–16116.
50. Lee, W.J., S.E. Lee & C.G. Kim. 2006. The mechanical properties of MWNT/PMMA nanocomposites fabricated by modified injection molding. *Compos. Struct.* **76:** 406–410.
51. Lewis, R., K.E. Asplin, G. Bruce, *et al.* 2011. The role of the membrane potential in chondrocyte volume regulation. *J. Cell. Physiol.* **226:** 2979–2986.
52. Eilers, P. & H. Boelens. 2005. Baseline Correction with Asymmetric Least Squares Smoothing.
53. Morales, T.I. 2007. Chondrocyte moves: clever strategies? *Osteoarthritis Cartilage* **15:** 861–871.
54. Albro, M.B., M.S. Bergholt, J.P. St-Pierre, *et al.* 2018. Raman spectroscopic imaging for quantification of depth-dependent and local heterogeneities in native and engineered cartilage. *npj Regen. Med.* **3:** 3.
55. Bonifacio, A., C. Beleites, F. Vittur, *et al.* 2010. Chemical imaging of articular cartilage sections with Raman mapping, employing uni- and multi-variate methods for data analysis. *Analyst* **135:** 3193–3204.
56. Byrne, H.J., K.M. Ostrowska, H. Nawaz, *et al.* 2014. Vibrational spectroscopy: disease diagnostics and beyond. *Chall. Adv. Comput. Chem. Phys.* **14:** 355–399.
57. Mansfield, J., J. Moger, E. Green, *et al.* 2013. Chemically specific imaging and *in-situ* chemical analysis of articular cartilage with stimulated Raman scattering. *J. Biophotonics* **6:** 803–814.
58. Frank, C.J., R.L. McCreary & D.C.B. Redd. 1995. Raman spectroscopy of normal and diseased human breast tissues. *Anal. Chem.* **67:** 777–783.
59. Movasaghi, Z., S. Rehman & I.U. Rehman. 2007. Raman spectroscopy of biological tissues. *Appl. Spectrosc. Rev.* **42:** 493–541.
60. Ziegler, L.D., Y.C. Chung, P. Wang, *et al.* 1989. Depolarization ratios of resonance Raman scattering in the gas phase. *J. Chem. Phys.* **90:** 4125–4143.
61. GOV.UK. 2021. Animals in Science Regulation Unit. Accessed Feb. 24, 2022. https://www.gov.uk/government/collections/animals-in-science-regulation-unit.
62. Giordani, S., S.D. Bergin, V. Nicolosi, *et al.* 2006. Debundling of single-walled nanotubes by dilution: observation of large populations of individual nanotubes in amide solvent dispersions. *J. Phys. Chem. B* **110:** 15708–15718.
63. Bergin, S.D., V. Nicolosi, P.V. Streich, *et al.* 2008. Towards solutions of single-walled carbon nanotubes in common solvents. *Adv. Mater.* **20:** 1876–1881.
64. Lin, C.-C. & K.S. Anseth. 2009. PEG hydrogels for the controlled release of biomolecules in regenerative medicine. *Pharm. Res.* **26:** 631–643.
65. Pedraza, E., A. Brady, C. Fraker, *et al.* 2013. Synthesis of macroporous poly(dimethylsiloxane) scaffolds for tissue engineering applications. *J. Biomater. Sci. Polym. Ed.* **24:** 1041–1056.
66. Westerlund, B. & T.K. Korhonen. 1993. Bacterial proteins binding to the mammalian extracellular matrix. *Mol. Microbiol.* **9:** 687–694.
67. Singh, B., C. Fleury, F. Jalalvand, *et al.* 2012. Human pathogens utilize host extracellular matrix proteins laminin and collagen for adhesion and invasion of the host. *FEMS Microbiol. Rev.* **36:** 1122–1180.
68. Hymes, J.P. & T.R. Klaenhammer. 2016. Stuck in the middle: fibronectin-binding proteins in Gram-positive bacteria. *Front. Microbiol.* **7:** 1504.
69. Yu, X., M. Cross, C. Liu, *et al.* 2012. Measurement of the traction force of biological cells by digital holography. *Biomed. Opt. Express* **3:** 153–159.
70. Dembo, M. & Y.L. Wang. 1999. Stresses at the cell-to-substrate interface during locomotion of fibroblasts. *Biophys. J.* **76:** 2307–2316.
71. O'Conor, C.J., N. Case & F. Guilak. 2013. Mechanical regulation of chondrogenesis. *Stem Cell Res. Ther.* **4:** 61.

72. Dinca, V., L.E. Sima, L. Rusen, *et al.* 2016. Bio-interfaces engineering using laser-based methods for controlled regulation of mesenchymal stem cell response *in vitro*. In *Recent Advances in Biopolymers*. F.K. Perveen, Ed.**:** 221–251. InTech.
73. Hu, J., C. Hardy, C.-M. Chen, *et al.* 2014. Enhanced cell adhesion and alignment on micro-wavy patterned surfaces. *PLoS One* **9:** e104502.
74. Sun, B., K. Xie, T.-H. Chen, *et al.* 2017. Preferred cell alignment along concave microgrooves. *RSC Adv.* **7:** 6788–6794.
75. Kim, Y., C. Kwon & H. Jeon. 2017. Genetically engineered phage induced selective H9c2 cardiomyocytes patterning in PDMS microgrooves. *Materials* **10:** 973.
76. Tijore, A., S.A. Irvine, U. Sarig, *et al.* 2018. Contact guidance for cardiac tissue engineering using 3D bioprinted gelatin patterned hydrogel. *Biofabrication* **10:** 025003.
77. Fodor, J., C. Matta, T. Oláh, *et al.* 2013. Store-operated calcium entry and calcium influx via voltage-operated calcium channels regulate intracellular calcium oscillations in chondrogenic cells. *Cell Calcium* **54:** 1–16.
78. Ma, B., J.C.H. Leijten, L. Wu, *et al.* 2013. Gene expression profiling of dedifferentiated human articular chondrocytes in monolayer culture. *Osteoarthritis Cartilage* **21:** 599–603.
79. Sato, E.T. & H. Martinho. 2018. First-principles calculations of Raman vibrational modes in the fingerprint region for connective tissue. *Biomed. Opt. Express* **9:** 1728–1734.
80. Huang, Z., A. McWilliams, S. Lam, *et al.* 2003. Effect of formalin fixation on the near-infrared Raman spectroscopy of normal and cancerous human bronchial tissues. *Int. J. Oncol.* **23:** 649–655.

Ann. N.Y. Acad. Sci. 1513 (2022) 48–64 © 2022 The Authors. *Annals of the New York Academy of Sciences* published by Wiley Periodicals LLC on behalf of New York Academy of Sciences.